



Nanoscopic evaluation of localized corrosion damages in an austenitic stainless steel

Komai K., Minoshima K.
Kyoto University, Japan

ABSTRACT This investigation demonstrates that an atomic force microscope (AFM) and a scanning tunneling microscope (STM) are capable of performing in-situ nanoscopic visualization of initiation and growth process of intergranular corrosion as well as stress corrosion cracking of an austenitic stainless steel. We discuss the concerned issues in an in situ SPM visualization in solutions and advantages and disadvantages of STM and AFM, as well as nanoscopic damage mechanisms based upon SPM observations.

INTRODUCTION

Most damage issues in machines and structures are caused by environmentally induced material degradation in an operating environment, including corrosion fatigue and stress corrosion cracking. In order to clarify the fracture and damage mechanisms of the environmentally induced material degradation, serial, high-magnification observations of damage initiation and growth processes are necessary. The traditional methods employed for such a purpose are scanning electron microscopy [1] and a measurement of microscopic distributions of corrosion current density, for example, by a scanning vibratory electrode technique [2,3]. In the former case, the test is periodically interrupted and the sample surface is examined in a completely different environment of vacuum from the testing environment, and therefore, an in situ or serial observation of changes in surface damage is impossible. This is because the exposure to vacuum affects the successive damage process, and the image obtained is quite different from the one in the testing environment owing to desiccation. Besides, the vertical resolution is insufficient for investigating the very early initiation stage of environmentally induced cracking and corrosion damage.

In contrast with these, a scanning tunneling microscope (STM), first developed in 1982 [4], gives a revolutionary tool to the study of surface physics and electrochemical researches [5-9]. It is capable of imaging nanoscopic topography of surface not only in vacuum but also in air or in

aqueous solutions. Although STM imaging of nonconducting surfaces is impossible, an atomic force microscope (AFM), that was developed in 1986 [10], can image topography of nonconducting surfaces [11]. Up to now, these microscopes are called scanning probe microscopes.

This investigation demonstrates that an atomic force microscope (AFM) and a scanning tunneling microscope (STM) are capable of performing in-situ nanoscopic visualization of initiation and growth process of intergranular corrosion as well as stress corrosion cracking of an austenitic stainless steel. We discuss the concerned issues in an in situ SPM visualization in solutions and advantages and disadvantages of STM and AFM, as well as nanoscopic damage mechanisms based upon SPM observations.

STM/AFM PROBE MICROSCOPES AND EXPERIMENTAL PROCEDURE

The principles of operation of an STM are very simple. An extremely, usually atomically, sharp conducting tip is brought in the proximity of a few nanometers from the sample surface. It is so

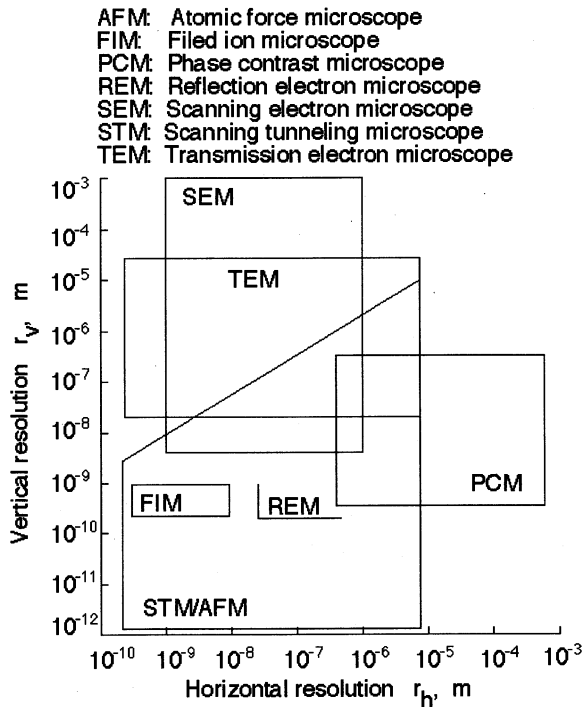


Fig. 1. Relation between horizontal and vertical resolution of various types of microscopes.

close positioned to the surface that a small constant voltage applied between the tip and the sample produces a electric current due to the tunneling effect. It is held constant by adjusting the z-axis of the micropositioner while the tip is raster-scanned. The image is formed from the record of vertical position required to keep the tunneling current constant as a function of x and y positions.

The traditional methods employed for measuring a topographic image are techniques based upon laser light, and/or a stereo-pair of images of electron microscopy. As contrast with these traditional methods, an advantage of an STM is its ultra-high resolution, in particular in the z direction.

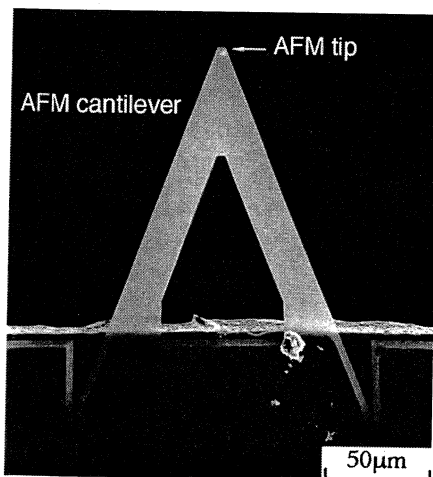


Fig.2(a). Micromachined cantilever in AFM system.

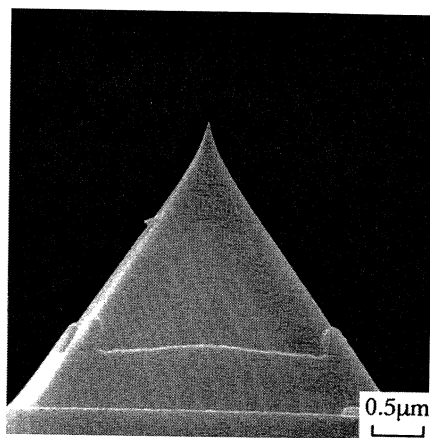


Fig.2(b). AFM tip of the cantilever in Fig. 2(a).

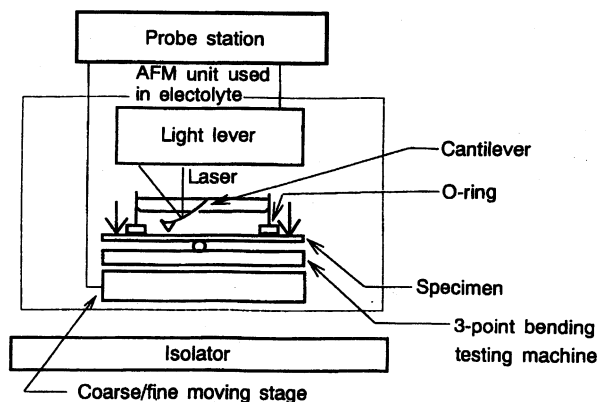
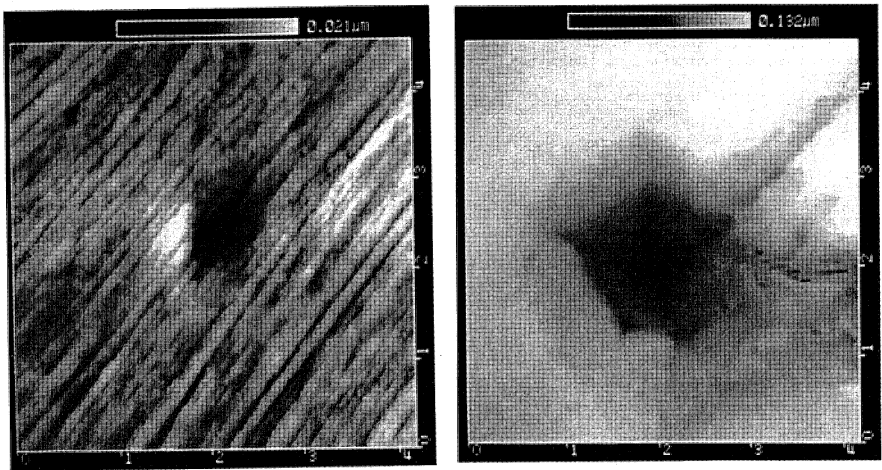


Fig. 3 Schematic of AFM system, equipped with specially designed small three-point bending device.

Figure 1 [12] summarizes the relation between horizontal and vertical resolution of several types of microscopes. It is clear that STM and AFM have very high resolution, in particular in the direction of depth. The dissipated power by tunneling current is about 1 pW to 10 nW, and therefore, the surface damage may be negligible. When the STM was developed, it was considered to operate only in vacuum. However, it is well known that it can operate not only in air but also in a solution. This is another advantage over traditional methods.

When an STM operates in a solution, we have to take account of the current due to electrochemical reactions on the tip that superimposes on the tunneling current: the current must be decreased by one-tenth to one hundredth of the tunneling current. For this purpose, an STM operating in a solution uses a special tunneling tip, which is insulated for all but the last few microns, to minimize the tip surface exposed to a solution, as well as a bi-potentiostat of four-electrode system, i.e., sample, counter electrode, reference electrode, and STM tip. Hence, the current associated with electrochemical reaction can be minimized.

A drawback of an STM is that it is not capable of imaging nonconducting surface, because the principle of STM is based upon the tunneling effect. However, a scanning probe microscope based upon another principle was developed, which can image not only conductive surface, but also nonconducting surface. This type of SPM is called an atomic force microscope (AFM). The cantilever used in an AFM (Fig. 2(a)) is of a micromachined Si_3N_4 or Si type. The sharp tip



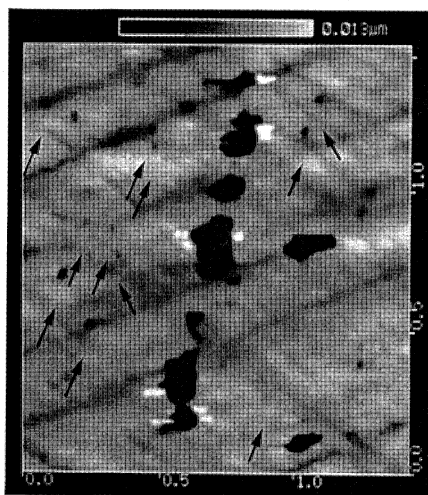
(a) Plastically deformed dent introduced by STM

(b) In situ visualization (Duration: 1h).

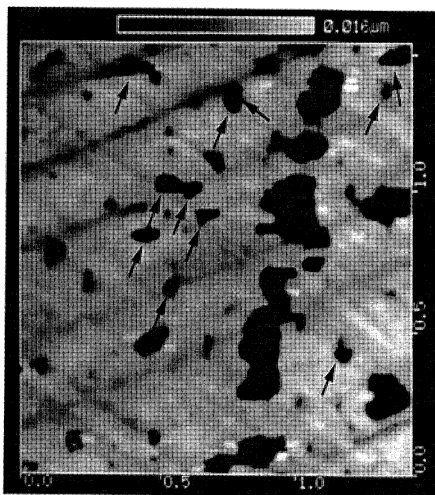
Fig. 4. In situ visualization of pitting corrosion of a sensitized austenitic stainless steel, SUS304, imaged by STM in a 3.5% NaCl solution. All dimensions are in μm .

(Fig. 2(b)) is positioned in the close proximity of the sample surface, thereby the cantilever being bent by the atomic force between the tip and the sample surface, because the spring constant of the cantilever is usually extremely small. By using the laser light lever, an image of topography is obtained by keeping the cantilever deflection constant. When an AFM was developed, the resolution was not so good as that of an STM. However, the resolution has been increased to an atomic scale, and it is not so difficult now to obtain atomic images by an AFM.

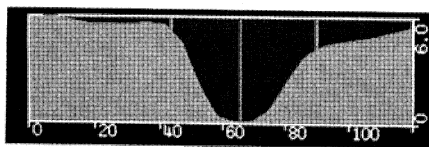
The schematic of the SPM system used in our laboratory is illustrated in Fig.3 [13,14]. The STM unit operating in air, the STM unit in solutions and the AFM unit operating in air and/or solutions are connected to the probe station, and in situ visualization can be performed in aqueous solutions. The individual unit was mounted on an isolator, and the probe station controls the operation of the units and the necessary image processing of the SPM images. The units are equipped with specially designed small three-point bending device, and in situ observation



(a) Immersion duration: 20 min.
All dimensions are in μm .



(b) Immersion duration: 31 min.
All dimensions are in μm .



(c) Cross section of pitting corrosion.
All dimensions are in nm.

Fig. 5. In situ visualization of pitting corrosion of a sensitized austenitic stainless steel, SUS304, imaged by AFM in a 3.5% NaCl + HCl solution (pH: 1.5).

under a constant displacement, or under loading, is possible.

IN SITU VISUALIZATION OF CORROSION PROCESS IN SOLUTION

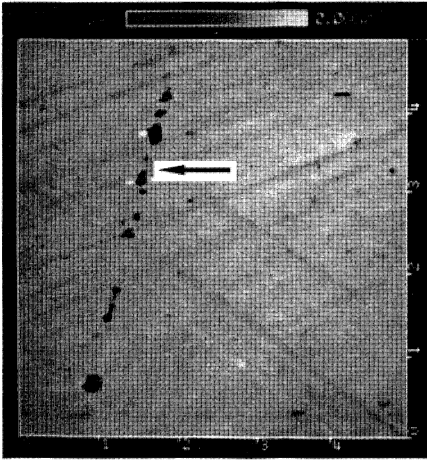
INSITU VISUALIZATION OF PITTING CORROSION

In situ visualization of a pitting corrosion process of a sensitized austenitic stainless steel (sensitization heat treatment: 650 °C for two hours) was performed by the STM [13]. The sample surface was indented in air by using the STM tip. Figure 4(a) illustrates the surface imaged by the STM operating in air, showing a plastically deformed dent of 1 μm in diameter and 20 nm in depth. Figure 4(b) shows the results of in situ STM visualization of the sample immersed in a 3.5 % NaCl solution after one hour immersion. This shows that corrosion concentrated in the area of plastically deformed zone, and the size of pitting corrosion became 2 μm in diameter and 130 nm in depth, which was still larger than the size of the initial dent. This means plasticity induced corrosion occurred around the dent.

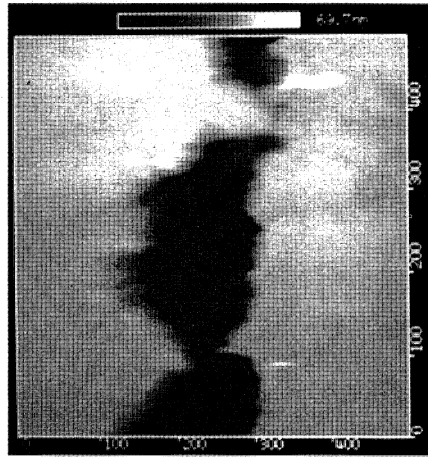
Figure 5 represents the AFM imaging of pitting corrosion of the sensitized stainless steel in a 3.5% NaCl + HCl solution (pH: 1.5). At immersion duration of 20 min (Fig.5(a)), not only large pitting along the grain boundary but also extremely small embryos of pitting shown by arrows could be seen. They were about 50 nm in diameter and 5nm in depth (Fig.5(c)). The pitting at immersion duration of 31 min that corresponded to the embryos observed in Fig.5(a) are shown by arrows in Fig.5(b). The embryos observed in Fig.5(a) grew to a relatively large, so-called pitting. This indicates that the extremely small embryos that could be seen at immersion duration of 20 min were the very early initiation stage of pitting corrosion: by using the AFM, the early initiation stage of pitting of the order of nanometer could be successfully visualized.

IN SITU VISUALIZATION OF INTERGRANULAR CORROSION

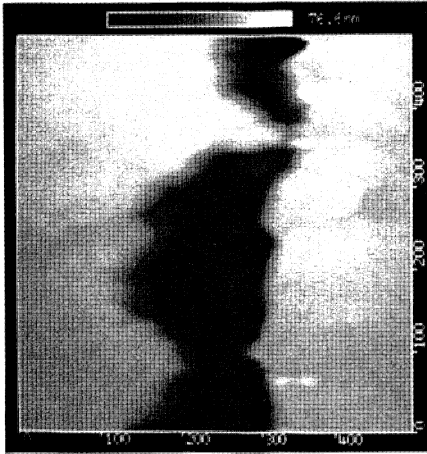
Figure 6 represents the in situ AFM visualization of intergranular corrosion process of the sensitized austenitic stainless steel in a 3.5% NaCl + HCl solution (pH: 1.5) [13]. Figure 6(a) is a low magnification image, and the site shown by an arrow was enlarged to nm scale. Figures 6(b) through (d) are serial, high-magnification images of the grain boundary area. These demonstrate that three aligned corrosion pits along the grain boundary of 80 nm in depth and 100 nm in diameter were coalescing with each other through the narrow groove between corrosion pits shown by arrows. These pits grew along the grain boundary, not in the depth (z) direction. These show that intergranular corrosion results from the coalescing of pitting corrosion aligned along a grain boundary. Figure 7 illustrates the birds'-eye view of Fig. 6, and the coalescing process is clearly visualized.



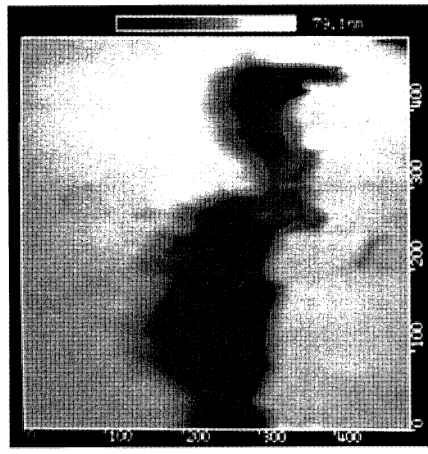
(a) General view,
Immersion duration: 18 min.
All dimensions are in μm .



(b) Immersion duration: 21 min.
All dimensions are in nm.

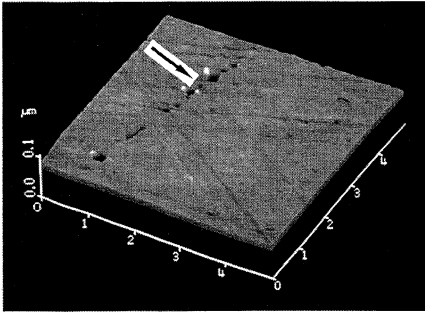


(c) Immersion duration: 24 min.
All dimensions are in nm.

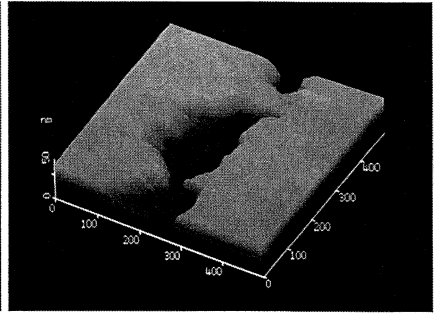


(d) Immersion duration: 29 min.
All dimensions are in nm.

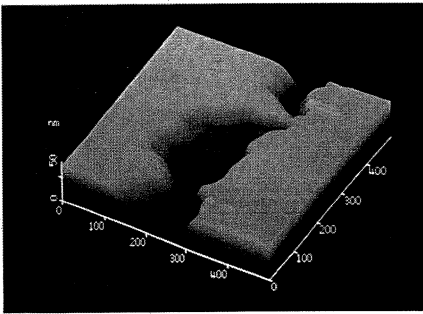
Fig. 6. In situ visualization of intergranular corrosion of an austenitic stainless steel, SUS304, imaged by AFM in a 3.5% NaCl + HCl solution (pH = 1.5).



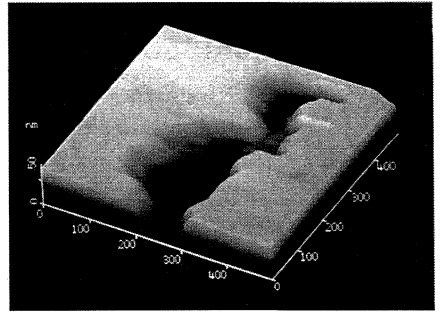
(a) General view, immersion duration : 18 min. All dimensions are in μm .



(b) Immersion duration: 21 min. All dimensions are in nm.



(c) Immersion duration: 24 min. All dimensions are in nm.



(d) Immersion duration: 29 min. All dimensions are in nm.

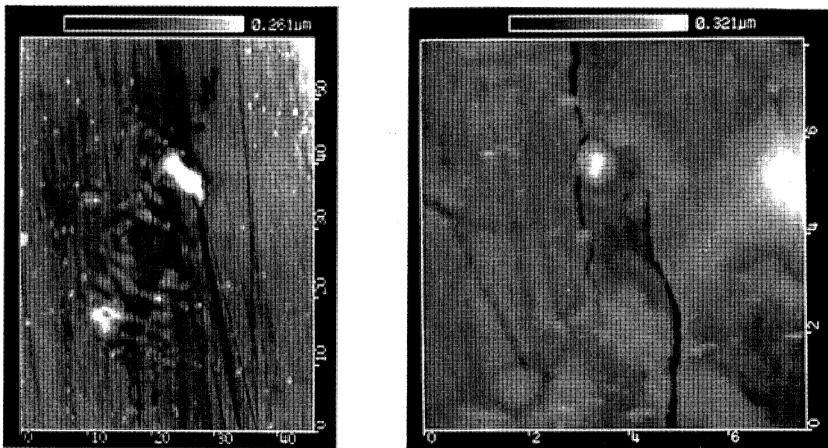
Fig. 7. Bird's-eye view of Fig. 6.

VISUALIZATION OF STRESS CORROSION CRACK GROWTH

Another interesting and useful application of SPM is an observation of growing, environmentally assisted cracking.

Visualization of stress corrosion (SC) crack of a sensitized austenitic stainless steel in a 30% MgCl_2 solution at 95 °C was performed[14]. The sample was mounted on the three-point bending jig, and was coated with silicon resin except the observing sample surface, in order to prevent the influence of galvanic corrosion on SC crack growth. The testing duration was 24h, and the applied maximum stress was 250MPa. Figure 8 shows the image of an SC precrack tip by using the STM in laboratory air. The SC crack tip restarted after it changed into pitting corrosion. Thereafter the branched SC crack tip preceded on the surface of the specimen as is shown in Fig.8(b).

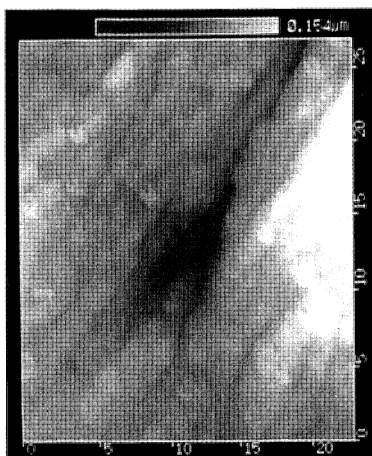
Figure. 9 shows a growing SC crack obtained by the AFM in air. The magnified image of Fig. 9(a) is illustrated in Fig. 9(b). In this case STM visualization was unable because of the deposited thick corrosion products. Almost all of the specimens surfaces in SCC tests was covered by the thick corrosion products, and STM observation was impossible. Though a single SC crack was identified in the observing area of 50 μm in Fig. 9(a), the crack was disconnected in the magnified Fig. 9(b). So much amount of corrosion products was deposited along crack lines, thereby proving intensified anodic corrosion reaction in the cracks.



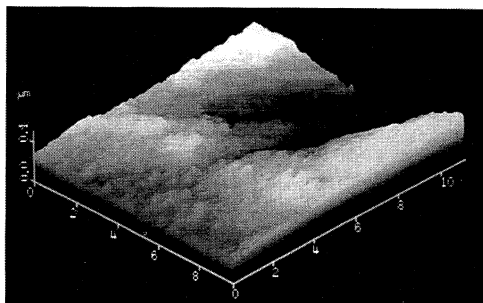
(a) Crack tip.

(b) Magnified topography of Fig.8(a).

Fig. 8. Visualization of SC crack of an austenitic stainless steel, SUS304, in a 30% MgCl_2 imaged by STM in air. All dimensions are in μm .



(a) Crack tip.



(b) Magnified image of Fig.9(a).

Fig. 9. Visualization of SC crack of an austenitic stainless steel, SUS304, in a 30% $MgCl_2$ imaged by AFM in air. All dimensions are in μm .

COMPARISON OF ADVANTAGE AND DISADVANTAGE OF STM AND AFM FOR IN SITU OBSERVATION

In this section, advantages and disadvantages of STM and AFM will be discussed. When an in situ observation is performed in a solution by using an STM, glass-insulated tip is necessary, and at the same time, the potential of the tip must be controlled: these techniques are used to decrease the electrochemical currents compared with the tunneling current. However, the glass coating was fragile, and serial imaging sometimes became impossible at a relatively early stage of an experiment. In contrast with this, no coating is necessary for the AFM tip, and such a problem can be avoided. Also no controlling the tip potential gives us simple operation procedures. This will make the very early stage observation after immersion possible. For STM, some operations are needed, and it is impossible to observe a sample surface just after immersion.

The next important point is that an STM is not capable of imaging non-conducting surface. This is because the operation principle is based upon the tunneling effects. When a corrosion process of a metal is observed, some nonconducting corrosion products are formed. In such a case, imaging the sample surface is impossible by using an STM. However, an AFM can image both conducting and nonconducting surfaces, and we do not have such problems. The tunneling

current is highly dependent on surface conditions, and scanning speed cannot be increased as an AFM can do: required time for imaging can be shortened by using an AFM.

Owing to the operation principle, the imaging of STM reflects the distribution of electron clouds, and therefore, the topography obtained by STM is not necessarily the outermost shape of surface. This is because the distribution of electron clouds is dependent on arrangements and bonding conditions of atoms as well as atom itself. Therefore, an artifact is seen in the STM image because of distribution of electron clouds. In contrast with this, all electrons including the outermost electrons contribute the AFM imaging, and therefore, it is considered that an AFM is capable of imaging the more faithful surface topography rather than using a STM [15].

As is discussed, an AFM is more suitable for performing in situ, serial visualization of corrosion process and observations of the fracture surface. An STM is suitable for basic research such as surface physics conducted in a precisely controlled, clean environment, such as ultra-high vacuum. This means that, from the technological viewpoints, an AFM has higher potential rather than an STM. However, attention must be taken to the shape of an AFM tip. Topography obtained by an AFM is influenced by a shape of a tip itself: further investigation is necessary, to establish standard AFM technique for observing sample surface.

CONCLUSIONS

The scanning probe microscopy (STM/AFM) is capable of imaging nanoscopic surface topography not only in vacuum, but also in air and solutions, and it is revolutionizing the study of surface physics and electrochemical researches. The SPM techniques are not only used for the researches on a corrosion process, growth behavior of stress corrosion cracking, but also for researches on initiation behavior of a fatigue crack [16, 17] and on degradation mechanisms of very small parts such as microelements used for micromachines [18]. To establish a standard method for performing in situ observation in air and/or in a solution by SPM and to integrate the SPM techniques with traditional techniques such as SEM will be a key technique to make a breakthrough in unsolved problems in the area of material strengths.

REFERENCES

1. Metals Handbook, Ninth Edition, Vol. 12, *Fractography* 1987., ASM International, .
2. Ishikawa, Y., & H.S. Isaacs 1983. Presented at Conf. Corros. and Expoliation of Aluminum Alloys, Cranfield, England, .
3. Minoshima, K. , S. Ogawa & K. Komai 1990. Proc. 11th Int. Corrosion Congress, 5: 477.
4. Binnig, G., H. Rohrer, C. Gerber, & E. Weibel 1982. Appl. Phys. Lett., 49: 57.
5. Sonnenfeld, R. & K. Hansma 1986. Science, 232: 211.

6. Lustenbelger, P., H. Rohrer, R. Christoph & H. Siegenthaler 1988. *Jour. Electroanal. Chem.*, 243: 225.
7. Itaya K. & E. Tomita 1988. *Surface Sci.*, 2: L507.
8. Masuda H., S. Matsuoka & N. Nagashima 1991. *Corro. Eng., Japan*, 40: 754.
9. Masuda H., N. Nagashima & S. Matsuoka 1991. *Trans. JSME, A*, 57: 2270.
10. Binnig G., C. F. Quate & C. Gerber 1986. *Phys. Rev. Lett.*, 56: 930.
11. Meyer G. & N. M. Amer 1990. *Appl. Phys. Lett.*, 56: 2100.
12. Kajimura K. 1986. *Nikkei Microdevice*, 11: 81.
13. Komai K., K. Minoshima & M. Itoh 1994. *J. Soc. Mater. Sci., Japan*, 43: 329.
14. Komai K., K. Minoshima & M. Itoh 1994. *J. Soc. Mater. Sci., Japan*, 43: 336.
15. Sakai A. 1995. *Sci. Machine*, 47: 638.
16. Ishii, H., S. Miyazu, K. Nakura & K. Tohgo 1993. *Trans. JSME, A*, 59: 3014.
17. Harvey S.E., P.G. Marsh & W.W. Gerberich 1994. *Acta Metall. Mater.*, 42: 3493.
18. Komai K., K. Minoshima, S. Inoue & H. Fujii 1995. *Trans. JSME, A*, 62: 978.